Towards a closed loop retinal prosthesis: measuring electrically evoked retinal responses using large electrodes

Journal of Neural Engineering

PAPER

Towards a closed loop retinal prosthesis: measuring electrically evoked retinal responses using large electrodes

Martin J Spencer[1,9,*], Suzanne Hosie[1,9], Wei Tong[2,6], Mohit N Shivdasani[3], David J Garrett[4], Sorel E De León[4], Emma K Brunton[1,6], Tatiana Kameneva[5], David B Grayden[1,6], James B Fallon[7,8], Michael R Ibbotson[1], Anthony N Burkitt[1,6] and Hamish Meffin[1,6]

[1] Department of Biomedical Engineering, The University of Melbourne, Parkville, Victoria, Australia
[2] School of Physics, The University of Melbourne, Parkville, Victoria, Australia
[3] Graduate School of Biomedical Engineering, University of New South Wales, Sydney, NSW, Australia
[4] School of Engineering, Royal Melbourne Institute of Technology, Melbourne, Victoria, Australia
[5] School of Science, Computing and Engineering Technologies, Swinburne University of Technology, Hawthorn, Victoria, Australia
[6] Graeme Clark Institute, University of Melbourne, Parkville, Victoria, Australia
[7] Bionics Institute, Carlton, Victoria, Australia
[8] Medical Bionics Department, The University of Melbourne, Parkville, Victoria, Australia
[9] Equal first authorship.
[*] Author to whom any correspondence should be addressed.

E-mail: martin.spencer@unimelb.edu.au

Keywords: retinal implant, stimulation strategies, suprachoroidal, neural stimulation artifact, compound action potential, closed loop

OPEN ACCESS

RECEIVED
27 November 2024

REVISED
4 August 2025

ACCEPTED FOR PUBLICATION
18 August 2025

PUBLISHED
29 August 2025

Abstract

Objective. Sensory prostheses use arrays of electrodes to stimulate neural tissue and restore a sense of vision or hearing. At perceptible levels of stimulation, the current from each electrode spreads and causes overlapping regions of neural activation. This lack of specificity results in perceptual deficits. Methods to overcome this reduced specificity, such as a closed loop stimulation approach require measurement of the neural response to stimulation. This investigation tests the possibility of using the large stimulating electrodes such as those required by some subretinal or suprachoroidal retinal implants to measure the neural response to stimulation, an approach similar to Evoked Compound Action Potentials measurements used in cochlear implants. *Approach. Ex vivo* tissue samples from Long Evans rats with healthy retinas and Royal College of Surgeon rats with retinal degeneration were used to investigate both stimulating and recording from electrodes of the same array. A hexagonal array was used with 20 platinum electrodes with 500 μm diameter and 700 μm pitch. Post-stimulus voltage decay was reduced with appropriate tuning of a triphasic stimulation pulse and in post-analysis with a high-pass filter. A method using alternating polarities of biphasic pulses was also trialed. A cocktail of synaptic and ion channel blockers was used to block all neural response including action potentials and thus confirm the biological origin of the signal. *Main Results.* It was found that a neural signal was observable on electrode that were sufficiently distant from the stimulating electrodes. The signal appeared to be due to direct activation of ganglion cells or possibly mediated via inner retinal neurons. *Significance.* This result confirms that recording usable neural signals from large electrodes is possible, which is an essential step in implementing a closed loop stimulation strategy for a subretinal or suprachoroidal retinal prosthesis.

1. Introduction

Neural prostheses use pulsed electrical currents to induce activity in neural tissue and restore functions such as hearing (Wilson and Dorman 2008), sight (Shepherd *et al* 2013), or bladder control (Fall and Lindström 1991) or to prevent pathological activity such as seizures (Fisher and Velasco 2014) or tremors (Krauss *et al* 2021). In each of these cases, more targeted electrical stimulation could increase efficacy and safety while reducing side effects.

Sensory prostheses such as cortical, cochlear, or retinal implants consist of arrays of electrodes that are electrically stimulated to induce useful sensory

perceptions of sound or light. At perceptible levels of stimulation there is a spread of neural activation from each electrode that overlaps with the neural activation created by neighboring electrodes (Wilke *et al* 2011, George *et al* 2015). This overlap creates a limitation on the potential benefit of high-density electrode arrays with increased numbers of electrodes.

Retinal prostheses treat conditions like Retinitis pigmentosa (RP), that lead to the degeneration of light sensitive cells. They may be located in an epiretinal (Sekirnjak *et al* 2008, Ho *et al* 2015, Luo and da Cruz 2016), subretinal (Stingl *et al* 2015), or suprachoroidal (Fujikado *et al* 2011, Ayton *et al* 2014, Bareket *et al* 2017) position. The suprachoroidal position maximizes surgical safety (Villalobos *et al* 2013) but it is most distal from the ganglion cells of the retina that are the target of the electrical stimulation. An array implanted in this suprachoroidal position typically requires higher stimulation currents combined with associated larger stimulation electrodes (Shivdasani *et al* 2014). Higher stimulation currents lead to wide overlapping spread of neural activation from each electrode (Sinclair *et al* 2016). These spreads of neural activation are associated with large phosphenes that do not allow perception of small visual features. Given that users of visual prostheses face significant limitations in on their ability to navigate or recognize objects (Karapanos *et al* 2021, Güven *et al* 2023) it is important to develop methods to overcome this effect.

Conventional strategies activate electrodes sequentially and aim to build perception of an image by combining the limited number of fixed phosphenes associated with the electrodes of the array (Chen *et al* 2009). This leads to poor vision outcomes, especially in sub-retinal and suprachoroidal implants, where the these phosphenes overlap, creating a low-resolution blurred effect (Wilke *et al* 2011, Sinclair *et al* 2016). The limit on visual acuity is the size of these phosphenes. More sophisticated 'current-steering' strategies attempt to improve this outcome by using multiple electrodes activated simultaneously. These focused multipolar or phased-array approaches synthesize a 'virtual' phosphene and manipulate its position and size to build an image sequentially (Frijns *et al* 2011, Spencer *et al* 2016, 2018). The use of the trans-impedance matrix to calculate the weights of each electrode as a proxy for neural activation is a limitation because it entails an implicit assumption that neural activation is a linear function of current. In reality, neural activations have nonlinear dependencies on electrode currents levels. It is likely that this is the reason that these strategies have not been widely adopted in the clinical setting.

It has been proposed that the negative effects of the conventional strategy and current-steering strategies could be overcome using a closed-loop approach (Guo *et al* 2018, Shah and Chichilnisky 2020, Tong *et al* 2020, Grani *et al* 2022) including a model-based neural activity shaping (NAS) algorithm (Spencer *et al* 2019, 2021, 2023, Castro *et al* 2024). Both solutions require measurement of neural responses, ideally via the electrodes of the stimulating array itself. These measurements must record the retinal response to electrical stimulation in the context of conditions such as RP.

The benefit of the proposed NAS strategy is that it uses these neural measurements to calculate an optimum simultaneous stimulation pattern to manipulate the pattern of neural activation (Spencer *et al* 2019). The perceived image is not built up of sequential phosphenes but is instead delivered in a 'single-shot'. This approach is likely to achieve higher acuity because the pattern of neural activation can be spatially sharpened using a push–pull approach between neighboring electrodes of opposite electrical polarity. This is possible because both linear, and non-linear neural activations are incorporated into the selection of the electrode current strengths and polarities. **Using NAS, the main limit on visual acuity is no longer individual phosphene size**, but instead, a less restrictive function of the electrode spacing (pitch), the accuracy of the neural response measurements, and the maximum electrode current (Spencer *et al* 2023). This higher acuity vision is expected to lead to significantly improved outcomes and higher quality of life for implantees. The present study represents a step towards this outcome by presenting evidence of the capacity of large electrodes to record an electrically evoked neural response.

There are existing studies that use small 6–25 μm electrodes in an epiretinal position to stimulate and record individual spikes using electrodes from the same array (Sekirnjak *et al* 2006, 2008, Madugula *et al* 2022). The present study investigates the possibility that the measurements of neural response could be performed by large 500 μm stimulation electrodes like those used in suprachoroidal implants. Under this proposal, one or more stimulation electrodes would be activated simultaneously and the resulting voltage fluctuations due to the combined neural response recorded. This is similar to the evoked compound action potential approach used in cochlear implants (Lai *et al* 2002).

Stimulation artifact is a notable obstacle to acquiring the neural signal. The stimulation artifact consists of both a direct recording of the voltage created by the stimulation pulse as well as the voltage decay (due to non-linear resistive-capacitive effects) following this pulse (Cohen *et al* 2003, Garcia *et al* 2021). Depending on the parameters of the recording apparatus, the decay artifact is approximately 100–1000 times larger than the neural response and so obscures the recording of the neural signal. In addition, the amplitude of neural signal is lower in the distal subretinal or suprachoroidal positions

compared to the proximal epiretinal position. If this decay artifact were significantly lower in frequency than the neural signal, it could be easily removed with a high-pass filter. However, large electrodes record the compound signal due to the spatial integration of the neural signals from many nearby neurons; this signal has lower frequency components than the higher frequency extracellular action potential recordings acquired with smaller electrodes.

The aim of this study is to determine whether measurement of electrically evoked ganglion cell signals in the retina is possible using large stimulating electrodes in a subretinal position. This result is essential in defining the steps necessary to develop a closed loop or activity shaping large-electrode retinal prosthesis. The result also has implications for other large-electrode stimulating arrays where NAS or closed loop approaches may be used.

2. Methods

This study was aimed at an initial characterization of the signals obtained from large electrodes in the retina, so measurements were undertaken using *ex vivo* retina tissue samples from rats. Rats have previously been used as a model for exploration of the efficacy of retinal implants (Kanda *et al* 2004, Ho *et al* 2019), including Royal College of Surgeons (RCS) rats which are a model of retinal degeneration (Strauss *et al* 1998, Pardue *et al* 2005).

A 2 mm × 3 mm hexagonal array was used to suit the size of rat retina tissue samples (figure 1(A)). The retina samples were placed in a subretinal orientation (figure 1(B)).

2.1. Electrode array

A hexagonal array was manufactured with four rows of five electrodes; 16 of these 20 electrodes were utilized during the experiment (figure 1(A)). The platinum electrodes had diameter 500 μm and pitch 700 μm. The array was embedded within a well that facilitated continuous perfusion of the retina with carbonated Ames' medium.

2.2. Retinal preparation

All experimental procedures were approved by the University of Melbourne Animal Ethics Committee (Ethics Approval #21886) and conformed to the policies of the National Health and Medical Research Council of Australia (NHMRC).

Retinas from 4 Long Evans rats (Animals #1-#4, 17–22 weeks old, all male) and 1 RCS rat (Animal #5, 21 weeks old, female) were used during the study.

Rats were initially anesthetized with a mixture of ketamine (100 mg kg)$^{-1}$ and xylazine (10 mg kg)$^{-1}$, and then humanely killed after retina dissection using intracardiac injection of Letharbarb (150 mg kg)$^{-1}$. Dissections were carried out in dim light conditions to avoid bleaching of photoreceptors.

Retinal preparations were carried out as described by (Maturana *et al* 2018). In brief, each eye was hemisected around the ora serrata, the vitreous body removed, and the eye cup inverted to detach the retina from the pigment epithelium. The retina was then divided into two or three segments and kept in a petri dish containing carbonated Ames' medium (Sigma-Aldrich) at room temperature until being placed on the array with ganglion cells facing up. An insulated tissue harp was used to hold the tissue in place.

2.3. Neural blockers

Pharmacological blockers were used when it was necessary to abolish neural signals. This was used to create a control condition in which identical stimulation protocols were performed before and after the application of blockers to determine the sources of recorded signals. A cocktail of blockers was used to remove all neural responses including the action potentials in ganglion cells. The blockers were added to the Ames perfusion medium with at least 40 min delay before new stimulations were performed.

NBQX (10 μM) was used to block AMPA/Kainate receptors. Strychnine (10 μM) was used to block glycinergic receptors. Picrotoxin 100uM was used to block GABA receptors. D-AP5 (50 μM) was used to block NMDA receptors. L-AP4 (20 μM) was to block mGluR6 receptors. This follows an approach used in a similar study (Zha *et al* 2023). In addition, Tetrodotoxin (TTX, 1.7 μM) was used to block sodium channels in retinal ganglion cells.

2.4. Stimulating and recording hardware

A Tucker-Davis Technologies 'IZ2' was used as the current stimulator and a Tucker-Davis Technologies PZ2 preamplifier was used as the voltage recorder (figure 1(C)).

The 'IZ2' can provide a maximum of 250 μA per channel. Multiple channels from the 'IZ2' were combined to provide higher current input to each electrode.

The 'PZ2' has a maximum input voltage of $\pm$10 mV. The recordings were obtained at a sample rate of 48.828 kHz. No in-line analogue filters were included in the recordings.

2.5. Electrical stimulation protocols

Stimulation was performed at a rate of 2 Hz on either a single electrode or three electrodes simultaneously. Clinically relevant current levels of up to 1500 μA were used (see discussion). In cases where three electrodes were used, the electric current listed is the total current across all three electrodes. For each parameter combination, multiple repetitions of stimulation pulses were delivered to allow for the removal of noise by averaging of the recorded signals. Animals #1-#3 and #5 used 80 repeats and animal #4 used 40 repeats for all measurements.

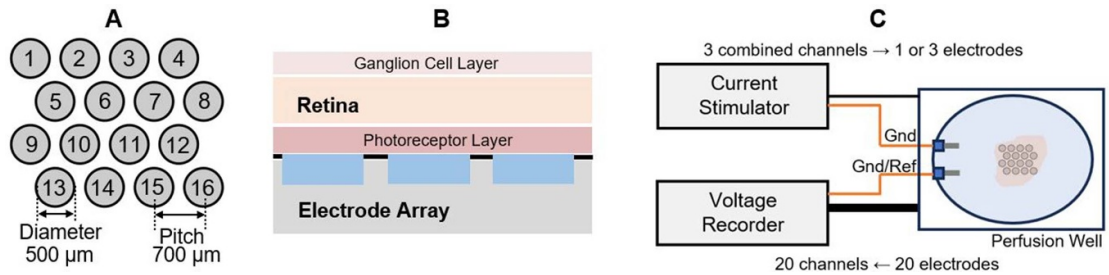

Figure 1. Dimensions of the electrode array used during the experiment and the position of the *ex vivo* retina on the array. (A) Electrode array size and topology. (B) Subretinal orientation of the *ex-vivo* retinal tissue sample on the electrode array. (C) Stimulator/recorder configuration during the measurements of neural response. Three channels of the Tucker-Davis technologies 'IZ2' were combined into single stimulation channel that was connected to either one or three electrodes to allow higher current stimulation. Voltages on all non-stimulating electrodes, were recorded by the 'PZ2'. The reference (Ref) and ground (Gnd) of the 'PZ2' were wired to a single electrode.

Unless otherwise stated, charge balanced triphasic pulses were used (figures 2(A)–(C)) that consisted of three phases: cathodic–anodic–cathodic (Bahmer *et al* 2010, Bahmer and Baumann 2012). Each phase was 500 μs in duration. The total charge delivered by the middle phase was balanced by the other two phases. The amplitudes of the first and third phases (α and $1-\alpha$) were adjusted to reduce the observed decay artifact (figure 2(C)). The values were chosen to be $\alpha = 0.62$ ($1-\alpha = 0.38$), based on a subjective evaluation of the most effective artifact removal, and these values were retained across all stimuli.

An alternative approach used biphasic pulses of opposite polarity (figures 2(D)–(F)). This is based on a technique originally described by (Abbas and Brown 1991). These consisted of two equal amplitude cathodic and anodic phases where each phase had a duration of 500 μs. To remove the decay artifact, two biphasic pulses were delivered with opposite polarity. By inverting the second pulse, the decay artifact's polarity was reversed while the neural signal's polarity was retained (blue and red traces in figure 2(F)). By averaging the resulting two recordings, the decay artifact could be removed, assuming an ideal linear response (black trace in figure 3(F)).

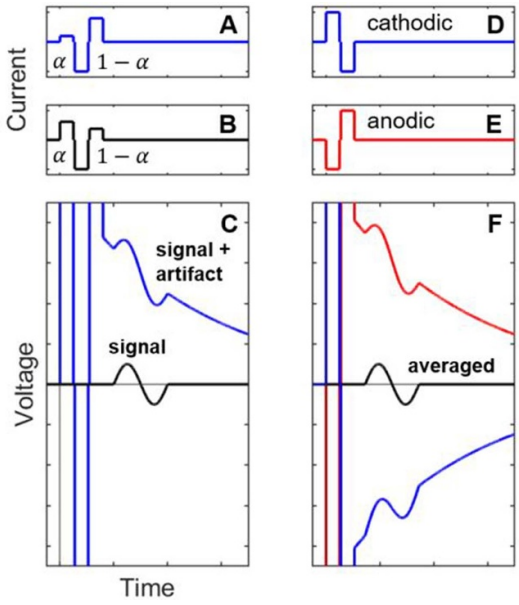

Figure 2. Stimulation protocols showing the methods used to reduce the electrical stimulation artifact amplitude and extract the neural signal. Left column: triphasic pulse stimulation. Right column: biphasic pulse stimulation. (A) Triphasic pulse with an untuned amplitude ratio. (B) Triphasic pulse with a tuned amplitude ratio. (C) Schematic depiction of the neural signal measured with an untuned pulse (blue trace) and a tuned triphasic pulse (black trace). (D) Biphasic pulse; cathodic phase first. (E) Biphasic pulse; anodic phase first. (F) Schematic depiction of the neural signal measured with a single biphasic pulse (blue and red traces) and an average measurement using two separate pulses of opposite polarities (black trace).

2.6. Light stimulation protocol

Light stimulation was used only to confirm the health of the *ex vivo* tissue and the capacity of the electrode array and recording apparatus to measure neural activation.

For this, a triggered laser with a wavelength of 488 nm and 275 mW peak power output was used with pulses of 0.1 ms. The laser light was passed through the lenses of a microscope, diffusing the light to cover the electrode array and tissue. The response to 8 pulses at 0.5 Hz were averaged and signals filtered with a 3rd order Butterworth lowpass filter with a cutoff of 150 Hz. The larger initial response to light for each stimulation trial series was discarded as it was often substantially higher amplitude than others.

2.7. Experimental procedure

The experimental procedure is shown in figure 3. During each experiment, the retina was dissected, prepared, and placed on the electrode array inside the perfusion well. The retina's response to light was confirmed, and then electrical stimulation and recording were undertaken. Blockers were then added to the perfusion fluid to eliminate any neural response. After waiting at least 40 min, electrical stimulation and recording were repeated as a control.

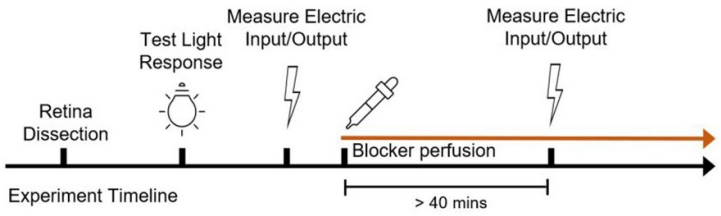

Figure 3. Schematic of experimental procedure timeline showing the sample preparation and confirmation of neural signal via light stimulation followed by the initial measurement of neural response before it was blocked using the cocktail of synaptic and channel blockers and then re-measured more than 40 min later.

2.8. Data analysis

After averaging the voltage recordings across repeated pulses, the final voltage waveform was band-pass filtered in the reverse time direction using a 3rd-order Butterworth filter with cutoffs of 5 Hz and 3500 Hz.

To calculate the amplitude of the neural response, a temporal window was chosen by visual inspection to exclude any decay artifact but retain the neural signal (shown as a grey region in figures 5, 6, and 7). This was chosen to be 3.5–10 ms post-stimulus from visual observation. The amplitude of the neural signal was defined to be the difference between the maximum and minimum voltage values within this window. This max–min approach was taken to exclude any voltage offset from the estimate of the neural signal amplitude.

3. Results

In this study, we considered a closed-loop sensory prosthesis whereby the same electrode array was used to stimulate and record neural activation simultaneously (Spencer 2024a, 2024b). The proximity of the stimulating and recording electrodes created large electrical artifacts that obscured the neural response. In quantifying the neural response, it was therefore important to account for the presence of any decay artifact resulting from stimulation.

3.1. Light stimulation

After placing the tissue, light stimulation was used to confirm its health and the correct operation of the recording apparatus. Increasing light intensity showed a response on all recording electrodes (Animal #3, figure 4(A)).

3.1.1. Triphasic pulse stimulation

Electrical stimulation was applied uniformly across either 1 or 3 electrodes. Recordings were made on all electrodes not used for stimulation (Animal #3, figure 4(B)). Different electrodes show a different level of artifact (grey arrows) and neural response later confirmed with blockers (green arrows).

It was found that with the recording apparatus used there were some recording electrodes that had a large exponential decay with or without the presence of blockers; electrode 9 for example (figures 5(B) and (E)). These artifact signals were not removed by adjustment of the value of α for the triphasic pulse (data not shown). Therefore, these electrodes were excluded from the analysis of the neural signal.

A second set of electrodes showed a response signal to electrical stimulation (figure 5(C)). Blockers were then introduced to remove all synaptic transmission as well as the direct activation of action potentials in ganglion cells. The signal was substantially removed by the addition of these blockers (figure 5(F)). This provides strong evidence that this signal is of neural origin. Furthermore, this signal was spatially localized (figure 5(A)). Other electrodes showed no response to stimulation before or after the addition of blockers to the perfusion (electrode 3, figures 5(D) and (G)). This collection of observations was consistent across all five animals.

Four wild-type rat retinas were tested for a neural response (figure 6). In each animal, there were large artifacts present in the recordings from the electrodes neighboring the stimulating electrodes. There was also a spatially localized neural response (figures 6(Ai)–(Di) and (Aii)–(Dii)). This signal was substantially removed by the addition of blockers (figures 6 (Aiii)–(Diii))

When the peak-to-peak amplitude of the neural response was plotted as a function of the stimulating electrode current, it was observed that the neural response showed a non-linear, sigmoid-like response with a threshold and saturation (figures 6 (Aiii)–(Diii)). This non-linear response is further indication of the neural origins of this signal. The reduced amplitude of the signal in animal #2 was possibly due to poor attachment of the retina to the electrode array.

The thresholds of approximately 250 μA (figures 6 (Aiii), (Biii), (Ciii) and (Diii)) correspond to a charge of 125 nC.

A frequency analysis of the data reveals that the neural signal has a frequency band of between 0 Hz and 400 Hz (figure 7). In addition, there is a peak for animal #1 at 120 $\pm$ 30 Hz (figure 7(A)) and animal #4 at 120 $\pm$ 30 Hz (figure 7(D)). Animal #2 and #3 have less clear peaks. Using the time between

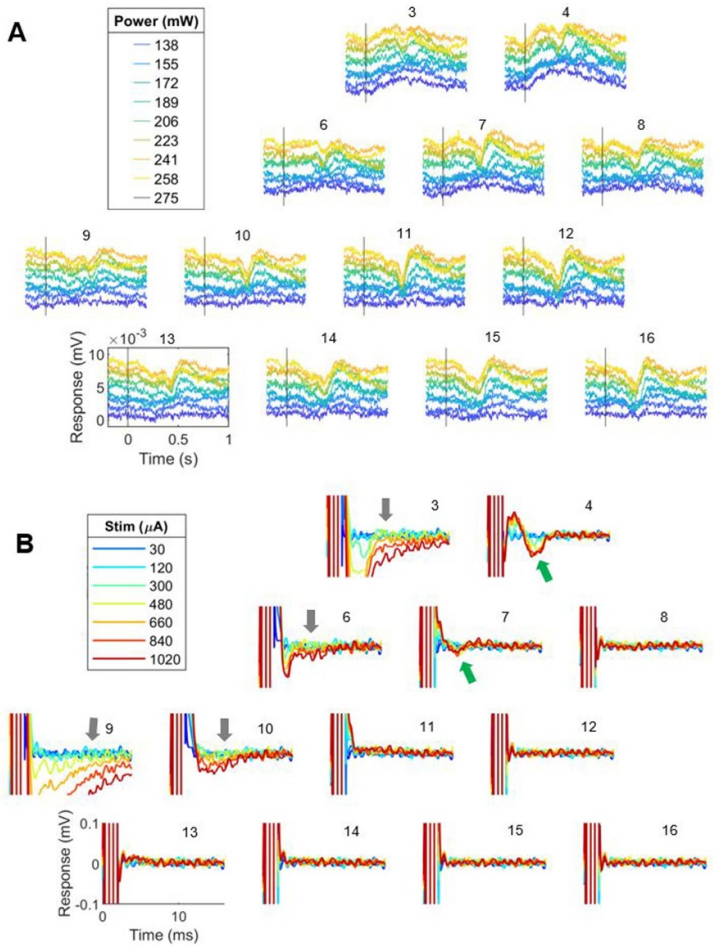

Figure 4. The response to light and electrical stimulation (Animal #3). Electrodes are numbered according to their positions in the array (refer to figure 1). Electrodes 1, 2, and 5 were used for electrical stimulation and so were not used for recording. (A) Response to a 0.1 ms flash of light of increasing intensity at a rate of 0.5 Hz. Colors indicate the power setting of the 488 nm laser used. Vertical black lines indicate the timing of the light stimulus. Note that small vertical offsets were added for visualization purposes. (B) Response to triphasic electrical stimulation at increasing currents. Colors indicate the total stimulation current used. Green arrows show likely neural response and black arrows indicate likely electrical artifact.

the minimum and maximum amplitudes in the time domain (figure 7) for each animal allows for an alternative estimate of the main frequency component of the signal of: animal #1 175 $\pm$ 25 Hz, animal #2 125 $\pm$ 25 Hz, animal #3 125 $\pm$ 25 Hz, animal #4 100 $\pm$ 25 Hz.

Retinal prostheses are used in cases of retinal degeneration. For this reason, the recordings were repeated with a retina from an RCS rat. A neural signal was observed with a similar spatial (figure 8(A)) and temporal (figure 8(B)) profile as the wild-type rats. This signal was also removed with the addition of blockers (figure 8(D)).

3.1.2. Biphasic pulse stimulation

The observations made in figures 4–8 were obtained using a tuned triphasic pulse approach to stimulation (figures 2(A)–(C)). This approach was taken to remove as much of the decay artifact as possible from the recordings. Although this was effective, it is known that this approach can require fine tuning of the pulse phase-weight parameter (α) to suppress the artifact with minor changes to the preparation or changes to the implant. For this reason, an alternative approach to removing the artifact was trialed using a pair of biphasic pulses of opposite polarity (figures 2(D)–(F)).

For both polarities, the neural signal in animal #4 in response to 1020 μA across the three stimulation electrodes (figure 6(Dii), orange trace) was substantially corrupted by a decay artifact (figure 9(A), catholic phase first—red trace, anodic phase first—blue trace). This decay artifact can be seen in the absence of a neural signal in the recordings taken after the addition of blockers (figure 9(C)). By averaging these recordings in response to stimulation of opposite polarities, the decay artifact was removed and the neural signal was revealed (figure 9(A), black trace). This signal was substantially removed by the addition of blockers (figure 9(C)), just as with the triphasic pulse approach. The method was applied at two stimulation currents before and after the addition

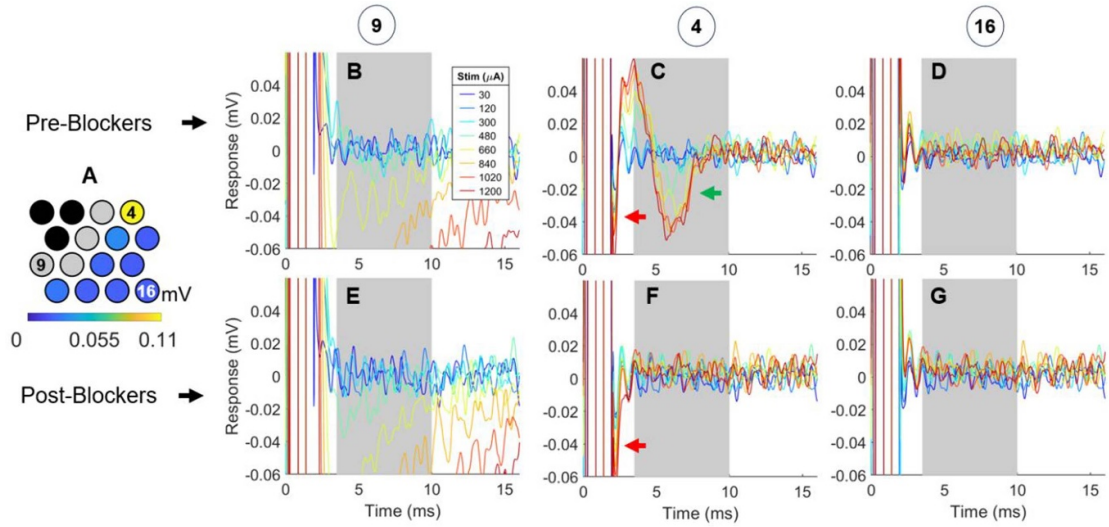

Figure 5. Recordings of neural response to electrical stimulation using triphasic pulses of varying current amplitudes (Animal #3). (A) Electrode array diagram with stimulating electrodes labeled black, electrodes with a large decay artifact labeled grey and the remaining electrodes colored according to the peak-to-peak amplitude of the neural signal. (B) Average post-stimulation response at different stimulation amplitudes recorded from an electrode with a large decay artifact (electrode 4 shown in A). (C) An electrode with a neural signal (electrode 4 shown in A). Green arrow indicates signal, red arrow indicates artifact. (D) An electrode with no artifact or neural signal (electrode 16 shown in A). (E)–(G) The same as (B)–(D) after the addition of blockers to the perfusion. In each of (B)–(G) the shaded area shows the temporal window used for the calculation of the amplitude of the response.

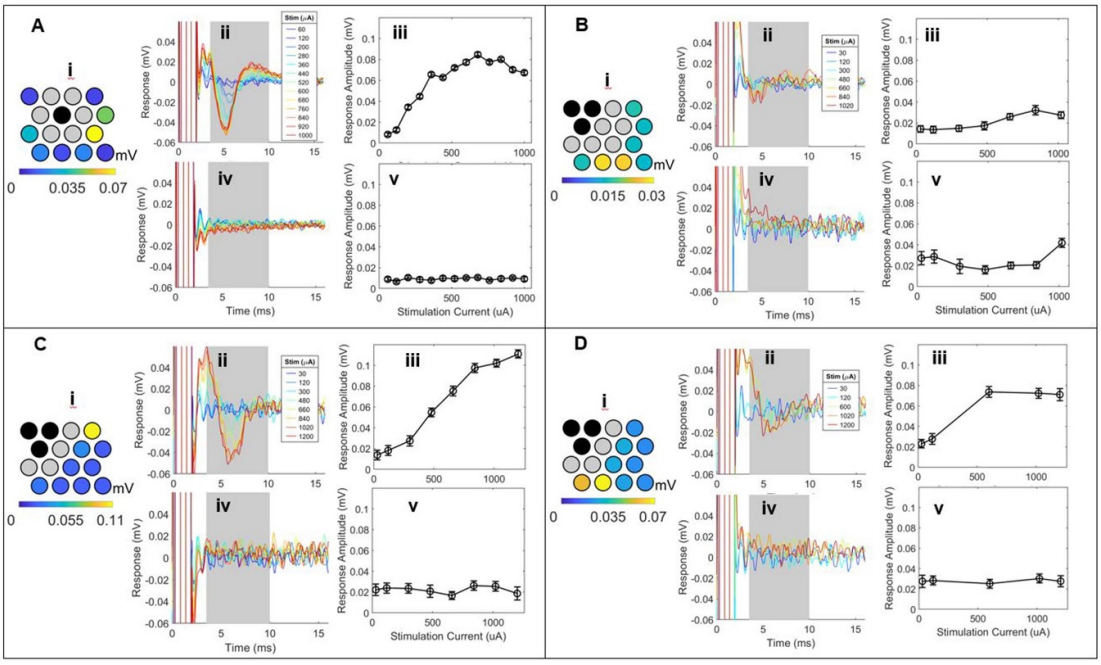

Figure 6. (A)–(D) Recordings of the response to electrical stimulation in four different animals (animals #1—#4, wild-type rats). (i) Electrode array diagram for each retina as described in figure 5 caption. (ii) Recording from the electrode with the highest amplitude neural response (yellow electrodes in *i*). The grey box shows the temporal region used during the calculation of the peak-to-peak amplitude of the neural signal. (iii) Input–output curve for the same electrode showing the peak-to-peak amplitude of the neural response as a function of the stimulation current. (iv) and (v) are the same as (ii) and (iii) after neural blockers were added to the perfusion. The error bars show the noise level that was calculated as the standard deviation in the signal for the same duration as the window but beginning 10 ms post-stimulus.

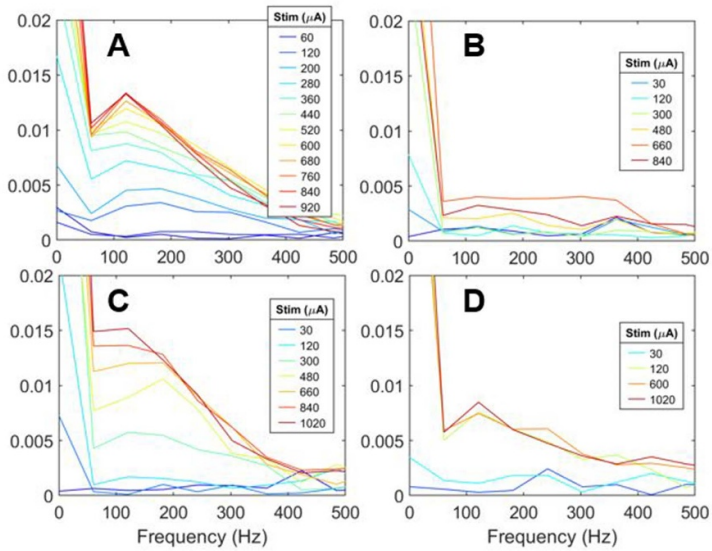

Figure 7. Frequency and spatial analysis of the neural signals shown in figure 6 ii using the data between 3.5 ms and 20 ms post-stimulus. Using a fast Fourier transform of the neural signals. (A)–(D) corresponds to each animal in figure 6(A)–(D).

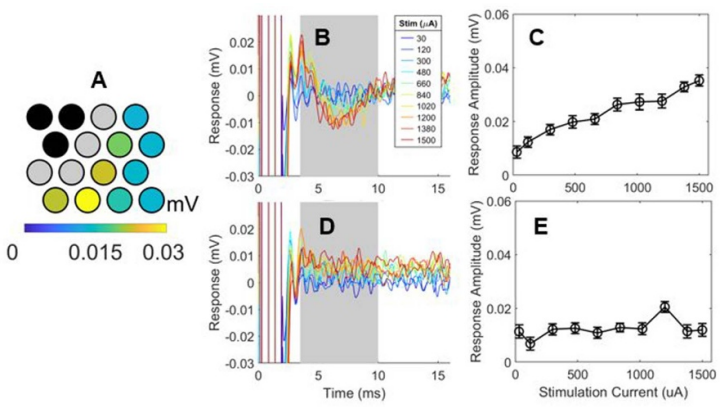

Figure 8. Recordings of the response to electrical stimulation in an animal with retinal degeneration (RCS rat). (A) Electrode array diagram showing the amplitude of the neural response. Stimulating electrodes (black). Large artifact (grey). (B) Recording from the electrode with the highest amplitude neural response (yellow electrode in A). (C) Input–Output curve showing the peak-to-peak amplitude of the neural response as a function of the stimulation current. (D) And (E) show the same results after the application of the combination of synaptic and ion-channel blockers.

of blockers (figure 9(B) and (D)). The difference with and without blockers can be easily observed (compare figures 9(B) and (D)).

4. Discussion

It was found that a retinal implant with large stimulating electrodes can successfully record a retinal response induced by stimulation using electrodes of the same array. This shows that there is a capacity to use the array in a closed-loop configuration or with a NAS algorithm.

Most *ex vivo* recordings involving electrically stimulated retina use patch-clamp recordings to record action potentials, see for example: (Maturana *et al* 2016). Previous *extracellular* recordings in response to electrical stimulating use small (10–30 μm diameter) electrodes positioned epiretinal (Sekirnjak *et al* 2006, 2008, Sekhar *et al* 2017, Madugula *et al* 2022). No previous work has examined the potential of measuring ganglion cell responses using much larger (500 μm) electrodes positioned sub-retinal. Investigating this possibility is important, given the superior safety profile of this position compared to epiretinal implantation.

The duration of the neural response (approximately 5 ms, figures 4–6) indicates that it was highly likely to be a compound action potential spatially averaged across a local population of retinal neurons. Furthermore, the short latency of the neural response ($<$ 5 ms, figures 4–6) indicates this likely originated from ganglion cells as a result of either their direct electrical stimulation or indirect activation by bipolar cells or a combination of both (Im and Fried 2015). It

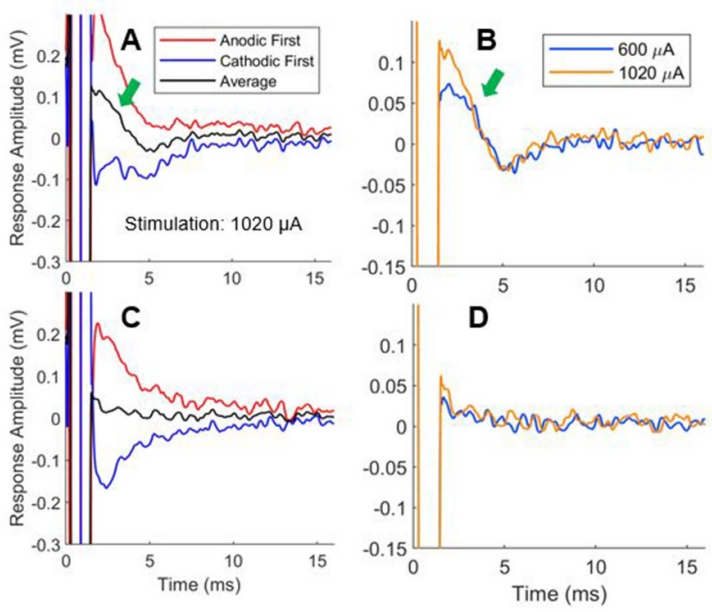

Figure 9. An alternative approach to artifact removal using biphasic stimulation with alternating polarity stimulation pulses as depicted in figure 2(D)–(F) (Animal #4, electrode 14). (A) Measured response before blockers added at an amplitude of 1020 μA. Red and blue curves show the response to biphasic pulses of opposite polarity. Black curve is the average of red and blue curves. Green arrow indicates neural signal. (B) Averaged alternating biphasic polarity results before blockers added at 600 μA and 1020 μA. Green arrow indicates neural signals. (C) After blockers added at an amplitude of 1020 μA. (D) After blockers added with stimulation of 600 μA and 1020 μA.

was unlikely to be due to photoreceptor activation. In future experiments specific blockers could be added in a sequence to isolate the contributions of various neuron types in the vertical processing pathway of the retina. In particular, it would be important to first block all synaptic input to ganglion cells to validate that there are no network contributions to the signal and finally using TTX block sodium channels in ganglion cells. This would provide strong evidence that the signal is likely from ganglion cells as a result of their direct activation.

Additional evidence that this signal was unlikely to be a result of photoreceptor activation was the threshold of its onset. The present study found the threshold to be approximately 125 nC. Activation of photoreceptors requires a lower charge given the suprachoroidal location of the implant. This is confirmed by comparison with the perceptual thresholds measured in the equivalent clinical device in human trials of a suprachoroidal retinal implant with a 500 μs phase duration; see figure 10(A) in (Shivdasani *et al* 2014) and (Petoe *et al* 2025).

The human suprachoroidal implant, with 1 mm diameter electrodes (Allen *et al* 2025) has a charge safety level of 745 nC (or 95 μC cm^{-2} calculated using the same approach as in (Shivdasani *et al* 2014), which used the Shannon model of safe levels for electrical stimulation (Merrill *et al* 2005). This corresponds to a current of 1500 μA; more than that used in the present study. This safe level of 745 nC is also 6 times the 125 nC thresholds measured in this investigation, giving confidence that the signals can be acquired clinically.

The choroid and retinal pigment epithelium (RPE) was not present in the preparations tested during this investigation, having been removed during dissection. Patients with retinitis pigmentosa are known to have substantially thinned choroid (Ayton *et al* 2013). However the presence *in vivo* of any additional choroid thickness will contribute to decreased signal to noise ratio (SNR) due to the modified electrical properties. In this study the distance from the electrodes to the ganglion cell layer was approximately 0.25 mm (Adachi *et al* 2016). In RP patients, due to the additional tissue, suprachoroidal implants are located approximately 0.3 mm from the ganglion cell layer (Ayton *et al* 2014, Yoon *et al* 2022). Due purely to the resistive properties of this additional ≈0.05 mm material the SNR will be decreased. Previous studies have assumed a purely resistive choroid (Joarder *et al* 2011) but additional capacitive or active properties may also reduce the SNR in a way that would differ on a patient-to-patient basis. The RPE may contribute some active response due to the presence of excitable cells. However, they will not introduce high-amplitude responses with similar frequency contributions in the same period of time as the signals measured. In an electroretinogram measurement for example the RPE contributes to the 'c-wave' which peaks after approximately 1 s (Audo *et al* 2008). These signal amplitudes are also reduced in conditions such as RP that lead to rod and cone cell degeneration.

The total effect of the presence of the choroid and RPE layer is something that should be investigated in future experiments *in vivo*. Given a SNR of 5 (figure 5(C) shows a peak-to-peak signal amplitude of 0.1 mV and peak-to-peak noise amplitude of 0.02 mV) a decrease in SNR is not anticipated to threaten the viability of the measurement.

In this investigation, artifact removal was achieved using a tuned triphasic pulse. In principle, if the baseline noise is sufficiently low, this method could use single-pulse recording. This is particularly advantageous in a closed-loop prosthesis that requires fast processing. Artifact removal using a biphasic alternating polarity protocol was also found to work using a pair of alternating polarity biphasic pulses. However, this approach, along with other approaches such as a mask-probe approach (Cohen *et al* 2003), require post-processing to extract the neural signal from the artifact.

It was not possible to record from the electrodes that were stimulated or the immediate neighboring electrodes due to the very large artifacts that saturated the recording amplifier. This was likely due to saturation of the recording amplifiers above ± 10 mV during stimulation (the limit of the TDT PZ2 amplifier). Improvements could be achieved using an amplifier with a higher maximum input voltage to allow for more accurate recording of the ≈ 100 μV neural signal amplitudes. These changes will likely allow recording from the immediate neighboring electrodes to the stimulating electrodes, or even from the stimulating electrodes themselves. The retinal response recorded by the stimulating array electrodes in response to full field high-intensity light stimulation was used in this study only to confirm the health of the retina and the functioning of the recording apparatus. To precisely measure the ganglion cell response to light requires particular specialized procedures (Porciatti 2015). For example, it is reported that stimulation at scotopic levels may reveal ganglion cell activity in an electroretinogram (Audo *et al* 2008). Such techniques were not performed in this study because the form of the neural signals obtained from light stimulation are likely very different to those obtained via electrical stimulation and so would not serve the purpose of informing us whether electrically evoked ganglion cell activity would be measurable with our setup.

Although rats are a previously used model for human vision in the context of retinal implant research (Kanda *et al* 2004, Ho *et al* 2015), it will also be important to verify that similar responses can also be recorded and characterized *in vivo* in larger animals prior to translating NAS for human application.

This study included results from only a single RCS rat and showed evidence for alternating polarity artifact removal from only a single rat at a limited number of current amplitudes. Further work is required to gather more evidence of the efficacy of the approach in degenerate retinas and with alternating polarity biphasic pulses.

The results of this paper demonstrate the potential for using large stimulating electrodes at relatively large distances from the retina for measurement of neural responses while simultaneously conducting electrical stimulation. Most retinal implants stimulate a population of retinal ganglion cells within a local area of the electrode. Given that the summed potentials we measure are likely from population that is local to that electrode, the signals are appropriate for the type of stimulation that is being applied. Given existing visual acuity is constrained by overlapping phosphenes, the measurements must simply obtain an estimate of the local neural activation at each electrode due to stimulation of neighboring electrodes.

The fact that signals could not be obtained from all electrodes is an impediment to obtaining the full forward model of electrical stimulation (which requires recording the response to simultaneous patterns of electrical stimulation). As noted above, modifications to the equipment is expected to allow greater artifact rejection. An additional approach is to spatially interleave stimulation and recording patterns to create multiple forward models that can then be merged into a single model.

Any increase SNR would impact the accuracy of the model, leading to a lower achievable increase in visual acuity via the NAS algorithm. The exact relationship also depends on other factors such as maximum safe electrode currents, and neural spread size; this is something that is explored explicitly in previous modeling studies (Spencer *et al* 2019, 2023). The SNR and spatial resolution of the measurements in the present investigation show that the necessary information to constrain this forward model is available.

In future *in vivo* experiments, spatial patterns of stimulation should be applied and recordings used to constrain a forward model (Maturana *et al* 2016). This fitted forward model can then be used to calculate optimal patterns of stimulation to induce particular neural activation in the form of spots and gratings (Spencer *et al* 2019). These patterns of neural activation could then be used to calculate the likely Snellen visual acuity (Spencer *et al* 2023) and compared to the visual acuity obtained via more conventional single electrode sequential stimulation.

Data availability statement

The data that support the findings of this study are openly available at the following URL/DOI: https://doi.org/10.17632/g4tbw5kfh9.1 and https://doi.org/10.17632/73972s5dpx.1.

Acknowledgment

This work was supported by the Australian Government through the National Health and Medical Research Council's Development Grant scheme [2014380], and the Australian Research Council's Discovery Projects funding scheme [DP220101166].

ORCID iDs

Martin J Spencer 0000-0002-2001-9054
Suzanne Hosie 0000-0002-4607-0800
Wei Tong 0000-0002-3725-2928
Mohit N Shivdasani 0000-0002-0692-4971
Sorel E De León 0000-0002-0227-2910
David B Grayden 0000-0002-5497-7234
James B Fallon 0000-0003-2686-3886
Anthony N Burkitt 0000-0001-5672-2772
Hamish Meffin 0000-0003-4307-6841

References

Abbas P J and Brown C J 1991 Electrically evoked auditory brainstem response: refractory properties and strength-duration functions *Hear. Res.* **51** 139–47

Adachi K, Takahashi S, Yamauchi K, Mounai N, Tanabu R and Nakazawa M 2016 Optical coherence tomography of retinal degeneration in royal college of surgeons rats and its correlation with morphology and electroretinography *PLoS One* **11** e0162835

Allen P J *et al* (for the Bionics Institute and Centre for Eye Research Australia Retinal Prosthesis Consortium) 2025 Second-generation (44-channel) suprachoroidal retinal prosthesis: surgical stability and safety during a 2-year clinical trial *Clin. Exp. Ophthalmol.* **53** 529–41

Audo I, Robson A G, Holder G E and Moore A T 2008 The negative ERG: clinical phenotypes and disease mechanisms of inner retinal dysfunction *Surv. Ophthalmol.* **53** 16–40

Ayton L N *et al* (for the Bionic Vision Australia Research Consortium) 2014 First-in-human trial of a novel suprachoroidal retinal prosthesis *PLoS One* **9** e115239

Ayton L N, Guymer R H and Luu C D 2013 Choroidal thickness profiles in retinitis pigmentosa *Clin. Exp. Ophthalmol.* **41** 396–403

Bahmer A and Baumann U 2012 Application of triphasic pulses with adjustable phase amplitude ratio (PAR) for cochlear ECAP recording: I. Amplitude growth functions *J. Neurosci. Methods* **205** 202–11

Bahmer A, Polak M and Baumann U 2010 Recording of electrically evoked auditory brainstem responses after electrical stimulation with biphasic, triphasic and precision triphasic pulses *Hear. Res.* **259** 75–85

Bareket L, Barriga-Rivera A, Zapf M P, Lovell N H and Suaning G J 2017 Progress in artificial vision through suprachoroidal retinal implants *J. Neural Eng.* **14** 045002

Castro D, Grayden D B, Meffin H and Spencer M 2024 Neural activity shaping in visual prostheses with deep learning *J. Neural Eng.* **21** 046025

Chen S C, Suaning G J, Morley J W and Lovell N H 2009 Simulating prosthetic vision: I. Visual models of phosphenes *Vis. Res.* **49** 1493–506

Cohen L T, Richardson L M, Saunders E and Cowan R S C 2003 Spatial spread of neural excitation in cochlear implant recipients: comparison of improved ECAP method and psychophysical forward masking *Hear. Res.* **179** 72–87

Fall M and Lindström S 1991 Electrical stimulation: a physiologic approach to the treatment of urinary incontinence *Urol. Clin. North Am.* **18** 393–407

Fisher R S and Velasco A L 2014 Electrical brain stimulation for epilepsy *Nat. Rev. Neurol.* **10** 261–70

Frijns J H M, Dekker D M T and Briaire J J 2011 Neural excitation patterns induced by phased-array stimulation in the implanted human cochlea *Acta Oto-Laryngol.* **131** 362–70

Fujikado T *et al* 2011 Testing of semichronically implanted retinal prosthesis by suprachoroidal-transretinal stimulation in patients with retinitis pigmentosa *Invest. Ophthalmol. Vis. Sci.* **52** 4726–33

Garcia C, Goehring T, Cosentino S, Turner R E, Deeks J M, Brochier T, Rughooputh T, Bance M and Carlyon R P 2021 The panoramic ECAP method: estimating patient-specific patterns of current spread and neural health in cochlear implant users *J. Assoc. Res. Otolaryngol. JARO* **22** 567–89

George S S, Shivdasani M N, Wise A K, Shepherd R K and Fallon J B 2015 Electrophysiological channel interactions using focused multipolar stimulation for cochlear implants *J. Neural Eng.* **12** 066005

Grani F, Soto-Sánchez C, Fimia A and Fernández E 2022 Toward a personalized closed-loop stimulation of the visual cortex: advances and challenges *Front. Cell Neurosci.* **16** 1034270

Guo T, Yang C Y, Tsai D, Muralidharan M, Suaning G J, Morley J W, Dokos S and Lovell N H 2018 Closed-loop efficient searching of optimal electrical stimulation parameters for preferential excitation of retinal ganglion cells *Front. Neurosci.* **12** 168

Güven D, Düzgün E, Kutucu O K and Gül C 2023 Evaluation of the long-term clinical results of 3 patients implanted with the Argus II retinal prosthesis *Turk. J. Ophthalmol.* **53** 58–66

Ho A C *et al* 2015 Long-term results from an epiretinal prosthesis to restore sight to the blind *Ophthalmology* **122** 1547–54

Ho E, Lei X, Flores T, Lorach H, Huang T, Galambos L, Kamins T, Harris J, Mathieson K and Palanker D 2019 Characteristics of prosthetic vision in rats with subretinal flat and pillar electrode arrays *J. Neural Eng.* **16** 066027

Im M and Fried S I 2015 Indirect activation elicits strong correlations between light and electrical responses in ON but not OFF retinal ganglion cells *J. Physiol.* **593** 3577–96

Joarder S A, Abramian M, Suaning G J, Lovell N H and Dokos S 2011 A continuum model of retinal electrical stimulation* *J. Neural Eng.* **8** 066006

Kanda H, Morimoto T, Fujikado T, Tano Y, Fukuda Y and Sawai H 2004 Electrophysiological studies of the feasibility of suprachoroidal-transretinal stimulation for artificial vision in normal and RCS rats *Invest. Ophthalmol. Vis. Sci.* **45** 560–6

Karapanos L *et al* 2021 Functional vision in the real-world environment with a 44-channel suprachoroidal retinal prosthesis *Invest. Ophthalmol. Vis. Sci.* **62** 3203

Krauss J K *et al* 2021 Technology of deep brain stimulation: current status and future directions *Nat. Rev. Neurol.* **17** 75–87

Lai W K, Müller-Deile J, Dillier N, Almqvist B, Stecker M, Frohne C and von Wallenberg E 2002 Measurement of the electrically evoked compound action potential via a neural response telemetry system *Ann. Otol. Rhinol. Laryngol.* **111** 407–14

Luo Y H-L and da Cruz L 2016 The Argus® II retinal prosthesis system *Prog. Retin. Eye Res.* **50** 89–107

Madugula S S *et al* 2022 Focal electrical stimulation of human retinal ganglion cells for vision restoration *J. Neural Eng.* **19** 066040

Maturana M I, Apollo N V, Garrett D J, Kameneva T, Cloherty S L, Grayden D B, Burkitt A N, Ibbotson M R and Meffin H 2018 Electrical receptive fields of retinal ganglion cells: influence of presynaptic neurons *PLOS Comput. Biol.* **14** e1005997

Maturana M I, Apollo N V, Hadjinicolaou A E, Garrett D J, Cloherty S L, Kameneva T, Grayden D B, Ibbotson M R and Meffin H 2016 A simple and accurate model to predict

responses to multi-electrode stimulation in the retina *PLOS Comput. Biol.* **12** e1004849
Merrill D R, Bikson M and Jefferys J G R 2005 Electrical stimulation of excitable tissue: design of efficacious and safe protocols *J. Neurosci. Methods* **141** 171–98
Pardue M T, Phillips M J, Yin H, Sippy B D, Webb-Wood S, Chow A Y and Ball S L 2005 Neuroprotective effect of subretinal implants in the RCS rat *Invest. Ophthalmol. Vis. Sci.* **46** 674–82
Petoe M A *et al* 2025 A second-generation (44-channel) suprachoroidal retinal prosthesis: a single-arm clinical trial of feasibility *Ophthalmol. Sci.* **5** 100525
Porciatti V 2015 Electrophysiological assessment of retinal ganglion cell function *Exp. Eye Res.* **141** 164–70
Sekhar S, Jalligampala A, Zrenner E and Rathbun D L 2017 Correspondence between visual and electrical input filters of ON and OFF mouse retinal ganglion cells *J. Neural Eng.* **14** 046017
Sekirnjak C, Hottowy P, Sher A, Dabrowski W, Litke A M and Chichilnisky E J 2006 Electrical stimulation of mammalian retinal ganglion cells with multielectrode arrays *J. Neurophysiol.* **95** 3311–27
Sekirnjak C, Hottowy P, Sher A, Dabrowski W, Litke A M and Chichilnisky E J 2008 High-resolution electrical stimulation of primate retina for epiretinal implant design *J. Neurosci.* **28** 4446–56
Shah N P and Chichilnisky E J 2020 Computational challenges and opportunities for a bi-directional artificial retina *J. Neural Eng.* **17** 055002
Shepherd R K, Shivdasani M N, Nayagam D A X, Williams C E and Blamey P J 2013 Visual prostheses for the blind *Trends Biotechnol.* **31** 562–71
Shivdasani M N, Sinclair N C, Dimitrov P N, Varsamidis M, Ayton L N, Luu C D, Perera T, McDermott H J and Blamey P J 2014 factors affecting perceptual thresholds in a suprachoroidal retinal prosthesis *Invest. Ophthalmol. Vis. Sci.* **55** 6467–81
Sinclair N C, Shivdasani M N, Perera T, Gillespie L N, McDermott H J, Ayton L N and Blamey P J (for the Bionic Vision Australia Consortium) 2016 The appearance of phosphenes elicited using a suprachoroidal retinal prosthesis *Invest. Ophthalmol. Vis. Sci.* **57** 4948–61
Spencer M J, Kameneva T, Grayden D B, Burkitt A N and Meffin H 2021 Neural activity shaping utilizing a partitioned target pattern *J. Neural Eng.* **18** 046025
Spencer M J, Kameneva T, Grayden D B, Meffin H and Burkitt A N 2019 Global activity shaping strategies for a retinal implant *J. Neural Eng.* **16** 026008
Spencer M 2024a Electrically Evoked In Vitro (Rat) Retinal Neural Responses Using Large (500 um) Stimulating Electrodes (ARCHIVE 1/2) *Mendeley Data* (https://doi.org/10.17632/g4tbw5kfh9.1)
Spencer M 2024b Electrically Evoked In Vitro (Rat) Retinal Neural Responses Using Large (500 um) Stimulating Electrodes (ARCHIVE 2/2) *Mendeley Data* (https://doi.org/10.17632/73972s5dpx.1)
Spencer M, Kameneva T, Grayden D B, Burkitt A N and Meffin H 2023 Quantifying visual acuity for pre-clinical testing of visual prostheses *J. Neural Eng.* **20** 016030
Spencer T C, Fallon J B and Shivdasani M N 2018 Creating virtual electrodes with 2D current steering *J. Neural Eng.* **15** 035002
Spencer T C, Fallon J B, Thien P C and Shivdasani M N 2016 Spatial restriction of neural activation using focused multipolar stimulation with a retinal prosthesis *Invest. Ophthalmol. Vis. Sci.* **57** 3181–91
Stingl K *et al* 2015 Subretinal visual implant alpha IMS—clinical trial interim report *Vis. Res.* **111** 149–60
Strauss O, Stumpff F, Mergler S, Wienrich M and Wiederholt M 1998 The Royal college of Surgeons rat: an animal model for inherited retinal degeneration with a still unknown genetic defect *Acta Anat.* **162** 101–11
Tong W, Meffin H, Garrett D J and Ibbotson M R 2020 Stimulation strategies for improving the resolution of retinal prostheses *Front. Neurosci.* **14** 262
Villalobos J *et al* 2013 A wide-field suprachoroidal retinal prosthesis is stable and well tolerated following chronic implantation *Invest. Ophthalmol. Vis. Sci.* **54** 3751–62
Wilke R G H, Moghadam G K, Lovell N H, Suaning G J and Dokos S 2011 Electric crosstalk impairs spatial resolution of multi-electrode arrays in retinal implants *J. Neural Eng.* **8** 046016
Wilson B S and Dorman M F 2008 Cochlear implants: a remarkable past and a brilliant future *Hear. Res.* **242** 3–21
Yoon C K, Bae K and Yu H G 2022 Longitudinal microstructure changes of the retina and choroid in retinitis pigmentosa *Am. J. Ophthalmol.* **241** 149–59
Zha M, Muralidharan M, Ly K, Guo T, Von Wegner F, Shabani H, Hosseinzadeh Z, Lovell N H, Rathbun D L and Shivdasani M N, 2023 Probing the contribution of vertical processing layers of the retina to white-noise electrical stimulation responses *2023 45th Annual Int. Conf. IEEE Engineering in Medicine & Biology Society (EMBC)*. pp 1–4